Computational and Structural Biotechnology Journal 18 (2020) 2259–2269

COMPUTATIONAL AND STRUCTURAL BIOTECHNOLOGY JOURNAL

journal homepage: www.elsevier.com/locate/csbj

Toward understanding the dynamic state of 3D genome

Soya Shinkai [a,*], Shuichi Onami [a], Ryuichiro Nakato [b,*]

[a] Laboratory for Developmental Dynamics, RIKEN Center for Biosystems Dynamics Research, Kobe 650-0047, Japan
[b] Laboratory of Computational Genomics, Institute for Quantitative Biosciences, The University of Tokyo, Tokyo 113-0032, Japan

ARTICLE INFO

Article history:
Received 18 June 2020
Received in revised form 11 August 2020
Accepted 12 August 2020
Available online 21 August 2020

Keywords:
3D genome organization
Hi-C
Polymer modeling
Polymer simulation
Microrheology

ABSTRACT

The three-dimensional (3D) genome organization and its role in biological activities have been investigated for over a decade in the field of cell biology. Recent studies using live-imaging and polymer simulation have suggested that the higher-order chromatin structures are dynamic; the stochastic fluctuations of nucleosomes and genomic loci cannot be captured by bulk-based chromosome conformation capture techniques (Hi-C). In this review, we focus on the physical nature of the 3D genome architecture. We first describe how to decode bulk Hi-C data with polymer modeling. We then introduce our recently developed PHi-C method, a computational tool for modeling the fluctuations of the 3D genome organization in the presence of stochastic thermal noise. We also present another new method that analyzes the dynamic rheology property (represented as microrheology spectra) as a measure of the flexibility and rigidity of genomic regions over time. By applying these methods to real Hi-C data, we highlighted a temporal hierarchy embedded in the 3D genome organization; chromatin interaction boundaries are more rigid than the boundary interior, while functional domains emerge as dynamic fluctuations within a particular time interval. Our methods may bridge the gap between live-cell imaging and Hi-C data and elucidate the nature of the dynamic 3D genome organization.

Contents

* Corresponding authors.
E-mail addresses: soya.shinkai@riken.jp (S. Shinkai), sonami@riken.jp (S. Onami), rnakato@iam.u-tokyo.ac.jp (R. Nakato).

https://doi.org/10.1016/j.csbj.2020.08.014

1. Introduction

The three-dimensional (3D) genome architecture plays a key role in diverse, intricately cooperating biological activities [1–3]. Mounting evidence suggests that the chromatin structure and concomitant intra- and inter-chromosome interactions are related to the proper regulation of transcription, replication, DNA damage repair, and cell differentiation [4–6]. The disruption of chromatin structures causes cancer and other diseases [7–9].

In the last decade, a plethora of studies have emerged that provide a mechanistic understanding of the role of chromatin interactions in genomic functions. This progress has been supported by the advancement of technology, including super-resolution microscopy, genome-wide chromosome conformation capture techniques (Hi-C), and *in silico* polymer simulation. The results of these studies suggested that chromosomes can be classified as belonging to either compartment A (regions with active transcription and open structures) or compartment B (largely inactive regions) [10]. Within these compartments, chromatin is further categorized into megabase-scale topologically associating domains (TADs) [11]. Recent experiments based on polymer simulation and *in vitro* systems support the idea that the higher-order chromatin structures such as TADs and enhancer-promoter loops are dynamic and can be partly explained by the "loop extrusion model," an active ATP-dependent process regulated by multiple factors such as cohesin, condensin, and CTCF [12–14].

In this review, we focus on the dynamic nature of chromosome structures, particularly from a physical perspective. We highlight our recently developed procedures for modeling the four-dimensional (4D) genome organization [15,16]. First, we provide a brief overview of polymer modeling of 3D genome organization. Second, we explain how the physical implications of Hi-C data can be decoded using polymer modeling. Next, we explain the unique points of our computational method, PHi-C [15], and compare it with other Hi-C data-driven polymer modeling methods. Then, we demonstrate the application of PHi-C analysis to Hi-C data with molecular perturbations. Finally, we propose a new interpretation of the dynamic 3D genome organization that can be used to understand Hi-C data better both physically and quantitatively.

2. Polymer modeling of chromatin for 3D genome organization

Chromosomes consist of long chromatin fibers packed inside the nucleus. Labeling of DNA within the nucleus and observation of its organization have led the field of chromosome biology since Walther Flemming described the rod-shaped structure of mitotic chromosomes [17]. Fluorescence *in situ* hybridization (FISH) technologies revealed that interphase chromosomes occupy distinct positions known as chromosome territories [18] and that labeled pairs of DNA sequences separated by 100–2000-kb are spatially distributed in interphase chromatin as polymers [19]. Therefore, polymer physical approaches, including polymer simulations, have been competent to uncover the nature of chromosome organization.

A polymer is a macromolecule consisting of N monomers subject to thermal fluctuations at the sub-micron scales [20]. The conformation of the polymer system is represented by the set of position vectors of monomers $\{\boldsymbol{R}_n\}_{n=0}^{N-1}$. In terms of physics, describing all interaction potentials in the polymer system is modeling the polymer and allows for theoretical analyses and simulations of the polymer dynamics and structure. For example, the polymeric connection between adjacent monomers is represented by the bonding potential $U_{\mathrm{bond}}(\boldsymbol{R}_n, \boldsymbol{R}_{n+1})$. Additionally, one can add M diffusive molecules, $\{\boldsymbol{r}_m\}_{m=0}^{M-1}$, interacting with the polymer system. Then, the potential $U_{\mathrm{polymer-molecule}}(\boldsymbol{R}_n, \boldsymbol{r}_m)$ can describe the interaction between a monomer of the polymer and a diffusive molecule.

Since Hi-C technology revealed the 3D genome organization within the nucleus, polymer modeling has bifurcated into two approaches: first-principles (or bottom-up, forward, mechanistic) models, and data-driven (or top-down, inverse, fitting-based) models [21–23]. The former consists of minimal physical assumptions and aims to reveal a set of minimal physical mechanisms underlying the 3D genome organization. In contrast, the latter uses Hi-C data as a constraint condition of the 3D genome organization and aims to reproduce the input Hi-C data and 3D conformations of the polymer model via an optimization procedure. In the next section, we focus on the latter modeling approaches to decipher Hi-C data. Here, we provide an overview of the historical results of the first-principles polymer models with simulations.

In 1998, using polymer modeling with simulations, researchers first evaluated how chromosome territories within the nucleus and the internal structure as a polymer were organized. The multiloop subcompartment model considered not only an excluded-volume interaction between monomers as a repulsive interaction but also subcompartments consisting of 120-kb loops [24]. The simulation results showed the formation of chromosome territories with separated chromosome arms, which agreed with experimental results regarding the radial density and position of genes. However, these results were derived from physical interaction potentials to correspond to experimental observations. In 2008, Rosa and Everaers presented simulations of a generic and minimal polymer model. Interestingly, the results showed that chromosome territories

Table 1
First-principles polymer models for 3D genome organization with simulations. U_{bond}, the bonding potential along the polymer backbone; $U_{\mathrm{repulsive}}$, the repulsive interaction potential between monomers and/or molecules of the system; $U_{\mathrm{territory}}$, the territory potential around each modeled polymer chain; U_{bend}, the bending potential along the polymer backbone; U_{loop}, the loop interaction potential between looping monomers; U_{HiC}, the interaction potential of the polymer inferred from Hi-C matrix; U_{nucleus}, the constraint potential from the nucleus structure; $U_{\mathrm{polymer-molecule}}$, the interaction potential between monomers of the polymer and diffusive molecules; $U_{\mathrm{attractive}}$, the attractive interaction potential between monomers of the polymer. These potentials are function of elements of the set $\left\{\{\boldsymbol{R}_n\}_{n=0}^{N-1}, \{\boldsymbol{r}_m\}_{m=0}^{M-1}\right\}$. The detailed forms of these potentials are slightly different with each modeling. SAW, self-avoiding walk.

Author (reference)	Interaction potentials	Main features	Year
Münkel & Langowski [24]	U_{bond}, $U_{\mathrm{repulsive}}$, $U_{\mathrm{territory}}$, $U_{\mathrm{loop(120-kb)}}$	Formation of chromosome territories with separated chromosome arms and multiloop subcompartments	1998
Rosa & Everaers [25]	U_{bond}, $U_{\mathrm{repulsive}}$, U_{bend}	Existence and stability of chromosome territories due to generic polymer effects	2008
Mateos-Langerak et al. [82]	U_{bond}, $U_{\mathrm{repulsive}}$, $U_{\mathrm{loop(random)}}$	Foloding of chromatin at 0.5–75 Mb length scales	2009
Tokuda et al. [83]	U_{bond}, $U_{\mathrm{repulsive}}$, U_{bend}, U_{HiC}, U_{nucleus}	Large fluctuation of the genome structure forming chromosome territories in the nucleus	2012
Barbieri et al. [26]	SAW polymer on a cubic lattice, binder affinity and concentration	Scaling properties of chromatin folding, Fractal state of chromatin, Processes of domain formation	2012
Brackley et al. [27]	U_{bond}, $U_{\mathrm{repulsive}}$, U_{bend}, $U_{\mathrm{polymer-molecule}}$	Clustering of DNA-binding proteins driven by the bridging-induced attraction	2013
Jost et al. [28]	U_{bond}, $U_{\mathrm{repulsive}}$, $U_{\mathrm{attractive}}$	Chromatin folding due to epigenetic-specific attractive interactions, Existence of different four phases: (i) coil, (ii) globule, (iii) microphase separation and (iv) multistability	2014
Fudenberg et al. [29]	U_{bond}, $U_{\mathrm{repulsive}}$, U_{bend}, $U_{\mathrm{loop(extrusion)}}$	Formation of TADs via active loop extrusion process limited by boundary elements	2016

spontaneously emerge due to the slow relaxation from the mitotic chromosome structure because of generic polymer effects [25].

After Hi-C technology was developed [10], novel genomic domains such as A/B compartments and TADs were identified, and the scaling law in 3D chromatin folding was revealed. The first-principles polymer modeling has attempted to determine the mechanism underlying chromatin domain formation according to the scaling law. The strings-binders-switch model was the first attempt to account for diffusive binding molecules interacting with sequence-specific chromatin-binding sites [26]. The binding molecules can bridge binding sites on chromatin and form dynamic chromatin loops via the molecules. This mechanism is known as bridging-induced attraction and can drive chromatin-induced phase separation [27,23]. Additionally, the binding effects were refined as epigenetically related attractive interactions between monomers of the block copolymer model [28]. These models suggest that sequence-specific chromatin-chromatin interactions contribute to the formation of dynamic loops and clusters in the 3D genome organization. Recently, the loop extrusion model suggested that the active loop extrusion process on chromatin dynamically forms TADs in concert with loop extruding and boundary factors [29]. Interestingly, the polymer simulations revealed the molecular roles of the chromatin architectural proteins, such as cohesin and CTCF. In the conclusion of this section, we summarize the remarkable features of the first-principles polymer models with their physical assumptions in terms of the interaction potentials (Table 1).

3. Polymer modeling of Hi-C data

3.1. How to describe contacts in polymer modeling

Chromosome conformation capture (3C)-based technologies detect genomic pair fragments that are in proximity to one another. Calculating a population-averaged Hi-C contact map requires a massive number of pairs from several million cells [30]. In this vast ensemble, the contact frequency between a DNA pair can be described as a probability. The binning resolution and matrix size of a contact map depend on the number of sequencing reads. Therefore, a dense contact matrix $\mathrm{C} = (C_{ij})$ at an appropriate resolution is ideal for quantitatively understanding the contact probabilities.

In Hi-C data-driven polymer modeling, we first model the polymeric chromatin fibers as successively connected beads, whose physical size is variable according to the binning resolution (Fig. 1A). Then, the contacts between the ith and jth beads are represented by certain conformations of the bead model (Fig. 1B). This model mimics the genomic contacts in 3C-derivative experiments. As FISH experiments have revealed conformational variety between two genomic loci in the cell nucleus, the distance between the ith and jth beads, d_{ij}, should be distributed in the conformation ensemble according to a probability density function $p(d_{ij})$. Additionally, to gather contributions of d_{ij} within the contact distance σ, here, we introduce a contact kernel function $f_\sigma(d_{ij})$ (Fig. 1C). Based on the above setting, in general, we can describe the contact probability between the ith and jth beads as

$$C_{ij} \propto \int_0^\infty f_\sigma(d_{ij}) p(d_{ij})\, \mathrm{d}d_{ij}. \tag{1}$$

This formula is a generalization of the relationship between FISH and 3C [31,32]. So far, in computational 3D genome modeling, the contact probability C_{ij} has been assumed to be a function of the spatial distance d_{ij} as follows [33]:

$$C_{ij} \propto d_{ij}^{-\alpha}. \tag{2}$$

However, this is an ad hoc relationship established for reconstructing 3D structures and lacks a physical basis.

Here, we provide a concrete functional form of Eq. (1). To calculate the integral, we need information for $f_\sigma(d_{ij})$ and $p(d_{ij})$. The former depends on the binning resolution of the Hi-C matrix, the physical size of the modeled beads, and the contact range represented by the contact distance σ for the modeled beads pair. Once we establish a physical assumption for the bead model, we can calculate the latter. To find a clue, we first started with a simple model, in which we adopt the bead-spring model and the Gaussian-type contact kernel function, $f_\sigma(d_{ij}) = \exp\left(-d_{ij}^2/(2\sigma^2)\right)$ [15]. The analytical calculation provided a formula

$$C_{ij} = \left(1 + \frac{\Sigma_{ij}^2}{\sigma^2}\right)^{-3/2}, \tag{3}$$

where Σ_{ij}^2 represents the variance for spatial conformations of the ith and jth beads and stems from the structural fluctuations of a chromosome in a thermal environment. Interestingly, this formula differs from Eq. (2). While Eq. (2) implies that the contact probability can be interpreted as a static distance, Eq. (3) states that the contact probability is a function of the variety of chromosome

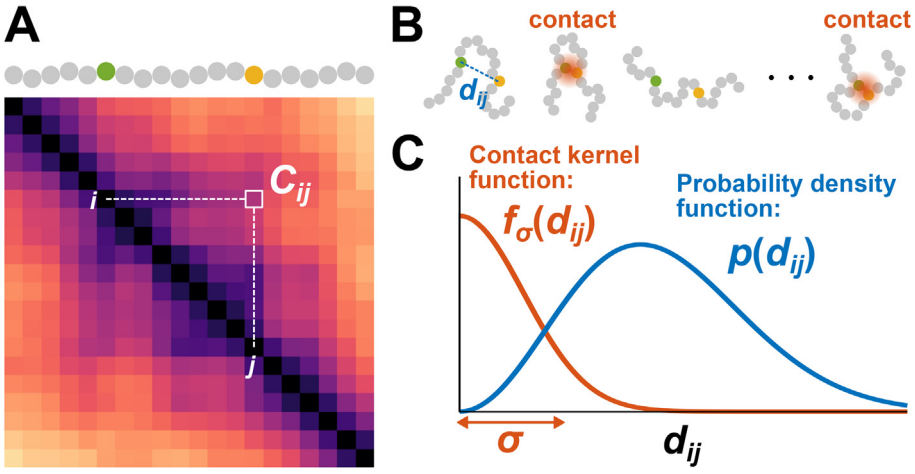

Fig. 1. Modeling the contacts in Hi-C experiments. A, Hi-C data are expressed as a heat map of the contact matrix $\mathrm{C} = (C_{ij})$ binned at an appropriate resolution. Corresponding to the binning, successively connected beads represent a toy polymer for the genomic region of interest. **B**, The contact between the ith and jth beads occurs in the proximity of the distance d_{ij}. **C**, The probability density function $p(d_{ij})$ represents a variety of the distance in polymer conformations. The contact kernel function $f_\sigma(d_{ij})$ gathers the contribution of the distances within the contact distance σ based on Eq. (1).

structures. Also, another contact kernel represented by the step function $f_\sigma(d_{ij}) = \theta(\sigma - d_{ij})$ states that C_{ij} is a function of the variance [34,35]:

$$C_{ij} = \mathrm{erf}\left(\frac{1}{\sqrt{2}\,\Sigma_{ij}/\sigma}\right) - \frac{\sqrt{2/\pi}}{\Sigma_{ij}/\sigma}\exp\left(-\frac{1}{2\,\Sigma_{ij}^2/\sigma^2}\right). \quad (4)$$

Notably, these theoretical expressions of the contact probability require the probability of the diagonal elements to be normalized as $C_{ii} = 1$.

3.2. Polymer modeling with network-like interactions can depict any contact pattern and simulate dynamic and structural features

Although Eqs. (3) and (4) have provided new mathematical insight into the contacts in Hi-C experiments, the quantitative interpretation of contact matrix data remains unclear. A useful polymer model allows us to simulate and predict the chromatin dynamics and structure in living cells from Hi-C data. To establish such a model, we need to include additional assumptions. However, as a minimal model, we need to limit the number of physical assumptions and parameters as much as possible. Handling $N \times N$-values of the contact matrix presents a problem, which can be addressed by mapping one contact matrix to another matrix through the relationship described in Eq. (3). Therefore, we introduced a polymer model with network-like interactions between two beads described by the interaction matrix $\bar{\mathrm{K}} = (\overline{K}_{ij})$ [15] (Fig. 2A). In terms of polymer physics, the positive or negative value of the matrix element $\overline{K}_{ij}$ represents the normalized intensity of attractive or repulsive interactions between the ith and jth beads, corresponding to the interaction potential $U_{ij} = \frac{1}{2}\overline{K}_{ij}(\boldsymbol{R}_i - \boldsymbol{R}_j)^2$. Then, we identified a one-to-one matrix transformation between the matrices $\bar{\mathrm{K}}$ and C. This transformation allows us to depict any contact pattern by setting the values of the interaction matrix.

As live-cell imaging experiments with single nucleosomes have revealed [36,37], the dynamic organization of chromatin domains occurs in a system experiencing stochastic thermal fluctuations, which inevitably drive the movements of the genome molecules present in the microscale cell environment. Polymer physics and polymer simulations are powerful ways to understand the relationship between chromatin dynamics and organization [38,39,21–23]. In our polymer modeling system, the interaction matrix $\bar{\mathrm{K}}$ also allows us to create simulations of 4D polymer dynamics featuring stochastic thermal fluctuations. With these simulations, we can conduct conformational sampling, calculate mean-squared displacement (MSD) curves of modeled monomers, and depict microrheology spectra [15,16] (Fig. 2B). Notably, the matrix $\bar{\mathrm{K}}$, which is the equivalent of an ensemble-averaged contact matrix, provides dynamics information. The 4D polymer dynamics simulation demonstrates the dynamic change in a modeled chro-

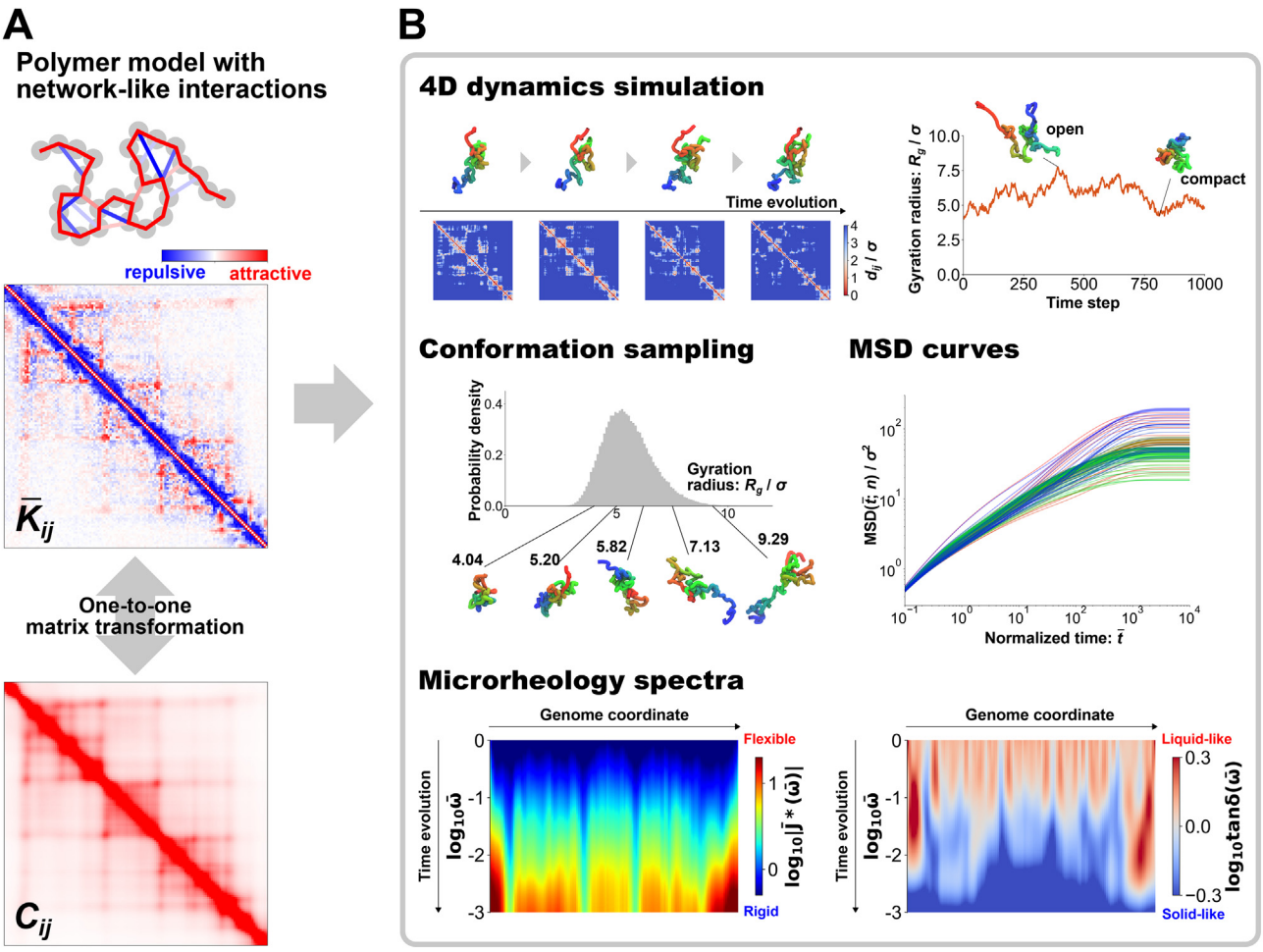

Fig. 2. Polymer modeling with network-like interactions bridges the gap between the genome dynamics and organization. A, Network-like attractive and repulsive interactions in a polymer model are expressed as a heat map of the interaction matrix $\bar{\mathrm{K}} = (\overline{K}_{ij})$. The one-to-one matrix transformation converts the matrix $\bar{\mathrm{K}}$ into a contact matrix $\mathrm{C} = (C_{ij})$. **B**, Based on the stochastic dynamics in thermal fluctuations, the matrix $\bar{\mathrm{K}}$ allows for 4D polymer dynamics simulations, sampling polymer conformations, mean-squared displacement (MSD) curves of modeled monomers, and microrheology spectra depictions.

matin fiber that occurs along with time evolution. For example, the simulation can reveal both open and compact structures embedded in the dynamics. Since the stochastic dynamics of the polymer model are ergodic [40], the time-averaged contact matrix in the dynamics coincides with an ensemble-averaged contact matrix consistent with the matrix $\bar{K}$. Furthermore, we can sample many polymer conformations in thermal equilibrium and quantitatively analyze the structural information such as the gyration radius. Moreover, recently, we developed a method, microrheology for Hi-C data, that can analyze the dynamic rheology property as a measure of the rigidity and flexibility of genomic regions along with the time evolution [16]. We can obtain a microrheology spectrum using the microrheology transformation formula [41] of the MSD curves derived from the matrix $\bar{K}$. The viscoelastic response to the periodic perturbation with a frequency ω is expressed as a heat map of a rheological quantity along two axes of the genomic coordinate and the frequency. The spectrum reveals the dynamic and hierarchical properties of the 3D genome organization embedded in the contact matrix.

The positive and negative interactions in the interaction matrix $\bar{K}$ imply that attractive and repulsive forces between two monomers do work. However, these forces should be thought of in theory as auxiliary, rather than as measurably real. Importantly, the matrix can be converted into measurable quantities such as the contact matrix, MSD curves, and dynamic rheological spectra. If these quantities predict the nature of chromosomes, the theory would be valid.

3.3. Deciphering Hi-C data by using the PHi-C optimization procedure

So far, we have explained the theoretical impacts of defining the contacts and Hi-C data-driven polymer modeling with the interaction matrix $\bar{K}$. We applied the theory to experimental Hi-C data to assess its validity. Mathematically, the inverse transformation from the contact matrix C to $\bar{K}$ might be sufficient to decode Hi-C data. However, this does not work well in practice because in experiments, we do not know the contact kernel function, there is experimental noise, and the number of sequencing reads might be insufficient for the ensemble-averaged contact matrix. Therefore, we developed an optimization algorithm for deciphering Hi-C data. Although other data-driven polymer models have also developed computational methods for finding optimized solutions to reconstruct 3D structures and contact maps [42–46,35], the molecular dynamics (MD) simulations and Monte Carlo (MC) sampling of polymer models have high computational costs associated with the optimization procedures. Conversely, in our method, we can determine the one-to-one matrix transformation needed to calculate a contact matrix C without the MD and MC simulations. This transformation could reduce the computational costs of optimization.

Fig. 3 summarizes the strategy and flowchart of our optimization procedure. First, we convert a temporary interaction matrix $\bar{K}_{\mathrm{Reconstructed}}$ into a contact matrix $C_{\mathrm{Reconstructed}}$ and compare it to an input Hi-C contact matrix $C_{\mathrm{Hi-C}}$ by using a cost function. Then, we slightly change the value of a randomly selected element of the interaction matrix and calculate the cost function. If the cost function decreases, we accept the change and update the interaction matrix. Practically, the cost function decreases with each iteration of these steps. Finally, we can obtain an optimized interaction matrix $\bar{K}_{\mathrm{Optimized}}$. Of note, another study used a similar strategy based on the Gaussian effective model (GEM) [34]. To complete the description of the procedure, we have to define the cost function in detail. The values of the contact probability are in the range of more than three orders of magnitude. Therefore, we might neglect the contributions of relatively fewer values by comparing two contact matrices in the linear scale. Thus, we compare two contact matrices in the logarithmic scale and use the Frobenius norm as the distance between them, as follows:

$$\begin{aligned}(\text{Cost function}) &= \sqrt{\frac{1}{N^2}\sum_{i=0}^{N-1}\sum_{j=0}^{N-1}\left|\log_{10}C_{ij}^{\mathrm{Hi-C}} - \log_{10}C_{ij}^{\mathrm{Reconstructed}}\right|^2} \\ &= \left|\left|\log_{10}C_{\mathrm{Hi-C}} - \log_{10}C_{\mathrm{Reconstructed}}\right|\right|_{\mathrm{F}}/N. \end{aligned} \quad (5)$$

Taken together with the simulation pipeline shown in Fig. 2, we developed a 4D simulation method, PHi-C (polymer dynamics deciphered from Hi-C data) [15]. Unlike other data-driven polymer modeling methods (Table 2), which also use experimental Hi-C data to obtain optimized physical parameters of the polymer model, PHi-C allows 2D Hi-C data to be interpreted as physical interaction parameters of the matrix $\bar{K}$ and 4D polymer dynamics consistent with dynamic features of the genomic loci observed in live-cell imaging experiments to be demonstrated.

3.4. Demonstration of PHi-C with microrheology analysis

Here, we will demonstrate how to decode Hi-C data by using PHi-C. The loop extrusion model is powerful enough to provide molecular mechanistic insight into how TADs are formed on chromatin through active molecular processes, and can also predict features of Hi-C maps by using molecular perturbations [29,47]. Also, recent Hi-C experiments have shown that condensin, cohesin, and CTCF as molecular candidates of the loop extrusion factors (LEFs) and the boundary elements (BEs) contribute 3D genome folding [48–50]. The depletion of cohesin release factor, Wapl, strengthened looping interactions at TAD boundaries due to an increase in cohesin processivity [51,52]. Loop extrusion polymer simulations taking into account the processivity of LEFs and the boundary strength of BEs predicted the consequences of cohesin, CTCF, and Wapl perturbations [47]. However, the parameters of the polymer model are not currently measurable within the living cell nucleus. Instead, we can determine the parameters of our polymer model in the PHi-C method through the optimization procedure. As long as the optimized contact map is in good agreement with the input experimental Hi-C matrix, the 4D simulations and microrheological features of our polymer model will be consistent with the Hi-C data. On the other hand, our polymer modeling cannot take into account active molecular processes.

Interestingly, without presuming that the modeling includes active processes, the PHi-C method depicts highly similar contact patterns for Hi-C data with perturbations to cohesin, CTCF, and Wapl [52] (Fig. 4A). These protein factors are thought to be necessary for the correct loop extrusion process in wild-type (WT) cells. Next, we applied our newly developed method, microrheology for Hi-C data [16], to characterize dynamic viscoelastic response property embedded in Hi-C data. As shown in Fig. 2, we converted each optimized interaction matrix $\bar{K}$ into the microrheology spectrum of complex compliance as a measure of the dynamic flexibility of the genome (Fig. 4B). The vertical stripe patterns were variable along the chromosome, suggesting that viscoelastic responses differed depending on the genomic region. The viscoelastic responses in boundary regions demarcating adjacent square areas on the contact matrices were relatively slower than those in the intra-square areas. As we have already reported, this indicates that TAD boundaries are more rigid as nodes than intra-TAD sequences [16].

We also compared the microrheology spectra of the Hi-C perturbation data to the spectra of WT cells (Fig. 4C). Cohesin degradation increases rheological mobility in a manner consistent with single-nucleosome dynamics in living cells [37]. Surprisingly, we observed white vertical stripes with ratio values of zero at the

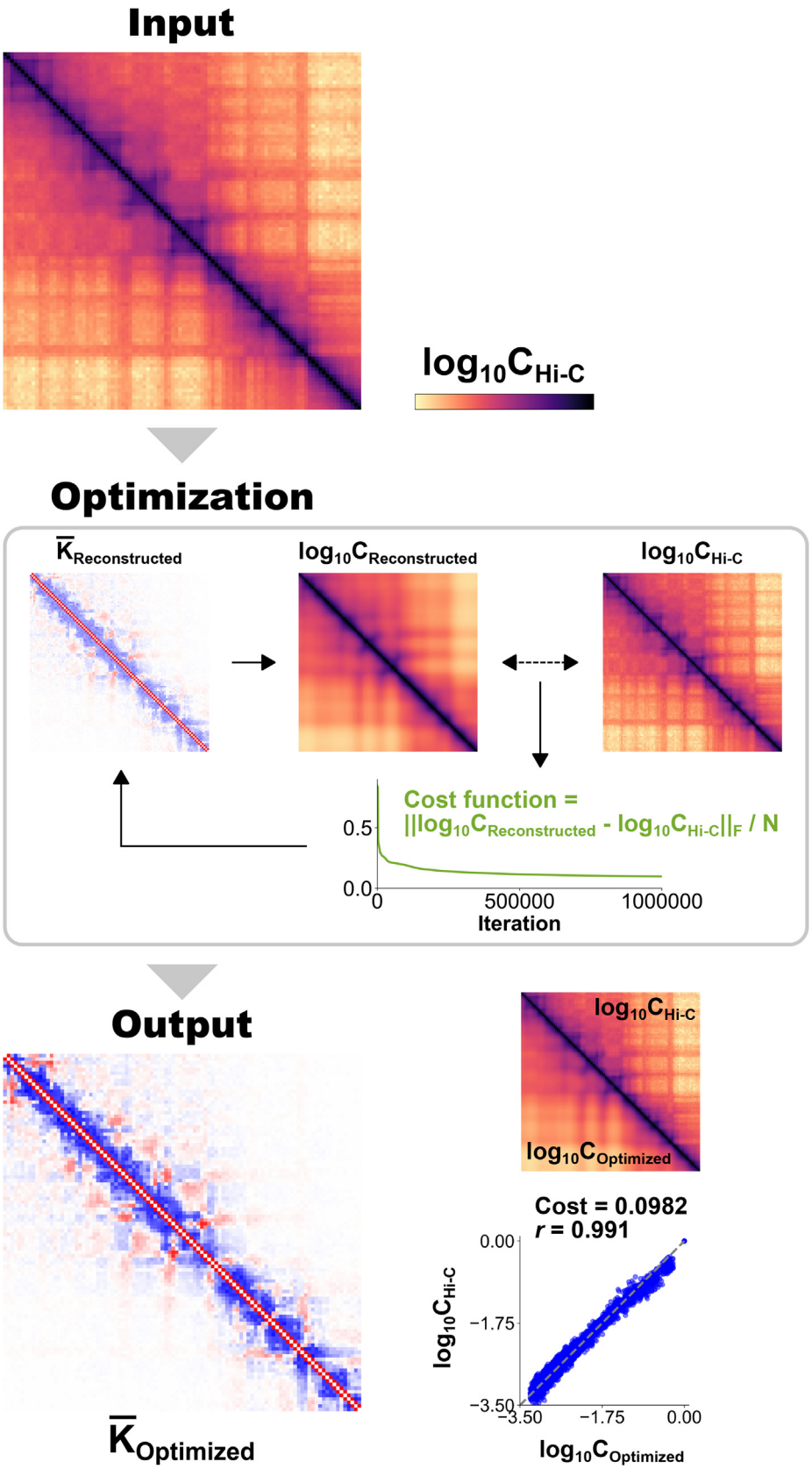

Fig. 3. PHi-C's optimization procedure outputs an optimized interaction matrix $\bar{K}_{Optimized}$ from an input contact matrix C_{Hi-C}. Iterative optimization steps update a temporary interaction matrix $\bar{K}_{Reconstructed}$ so that the difference between the contact matrices $C_{Reconstructed}$ and C_{Hi-C} in the logarithmic scale decreases.

Table 2
Data-driven polymer modeling methods reconstructing the input Hi-C matrix. The average Pearson's correlation values were calculated from Pearson's correlation values to compare experimental and reconstructed contact matrices in each paper.

Method	Average Pearson's correlation	Comparison between Hi-C matrices	Output models	Available from
MiChroM [44]	0.956	C_{Hi-C} and $C_{Reconstructed}$	3D structures	
PRISMR [46]	0.93	C_{Hi-C} and $C_{Reconstructed}$	3D structures	
GEM [34]	0.91	C_{Hi-C} and $C_{Reconstructed}$	4D dynamics	https://github.com/gletreut/gem_reconstruction
HLM [35]	0.955	Selected contact pairs	3D structures	
PHi-C [15]	0.960	$\log_{10}C_{Hi-C}$ and $\log_{10}C_{Reconstructed}$	4D dynamics	https://github.com/soyashinkai/PHi-C

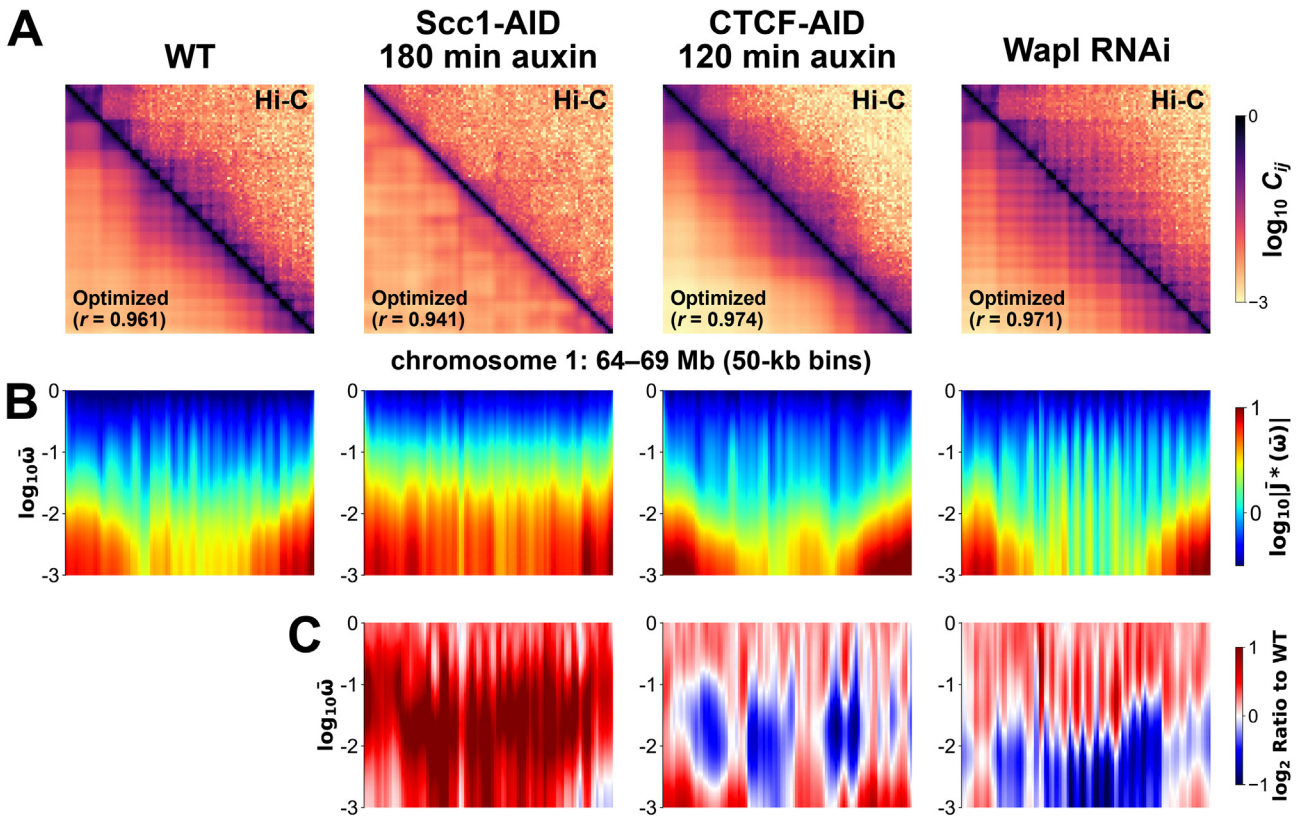

Fig. 4. PHi-C method deciphers Hi-C data with perturbations to cohesin, CTCF, and Wapl. A, Experimental (upper right triangle) and optimized (lower left triangle) contact matrices for HeLa cells (WT), auxin-induced SCC1 degradation cells, auxin-induced CTCF degradation cells, and Wapl RNAi cells [52]. SCC1 is a cohesin subunit. As a demonstration, we focused on the 64- to 69-Mb genomic region of chromosome 1 at 50-kb resolution. We observed high values for Pearson's correlation coefficient, *r*, between the optimized matrices and each input Hi-C matrix. We used the contact kernel function by Eq. (4) in the PHi-C optimization. **B**, Microrheology spectra of complex compliance, $|\bar{J}^*(\bar{\omega})|$, as a measure of the dynamic flexibility of four cases. The inverse of the frequency $\bar{\omega}$ corresponds to a time scale. **C**, Maps of the ratio between the microrheology spectra of Hi-C data and the spectra of WT data.

boundaries of the square areas on Hi-C maps of CTCF and Wapl depletion cases, suggesting that the dynamic rheological properties of the boundaries changed very little. Red regions with positive ratio values inside domain boundaries revealed the enhancement of rheological mobility, which heightens inter-domain interactions. As a result, the insulation ability at the boundaries may decrease; it has been reported that CTCF depletion disrupts the insulation of neighboring TADs [49,50]. Blue regions with negative ratio values showed a more rigid response with a time scale that corresponded to the inverse of the frequency $\bar{\omega}$. As Wapl-deficient cells accumulate contact at multi-TAD corners [52,51], chromatin formation becomes more compact. The compaction may increase the rheological rigidity of the nested interaction regions.

4. Emergence of chromatin domains in systems with dynamic fluctuations

There are two novel features present in the PHi-C modeling method. First, the PHi-C optimization procedure provides the full parameter set of the polymer model with network-like interactions, which can be used to reconstruct an input Hi-C contact matrix. Notably, here, inferring 3D genome structures by using the relationship between the contact probability and the pairwise distance (Eq. (2)) is not necessary for understanding Hi-C data in terms of polymer physics. Second, PHi-C's 4D simulations and microrheology spectra enable us to interpret ensemble-averaged Hi-C data as dynamic information, since the stochastic dynamics of the polymer model in thermal equilibrium satisfies ergodic properties [15,16,40]. Fig. 5 shows the snapshots of polymer conformations and the associated distance maps at each conformation in a 4D PHi-C simulation. Although it is difficult to find globular domains among the conformations and stationary high-contact triangles on the distance maps, time-averaging the contacts in the dynamics yields a time-averaged contact matrix equivalent to the ensemble-averaged contact matrix, due to the ergodicity of the stochastic dynamics.

This dynamics-based perspective can be used to amend the conventional perspective of the 3D genome organization. Recent

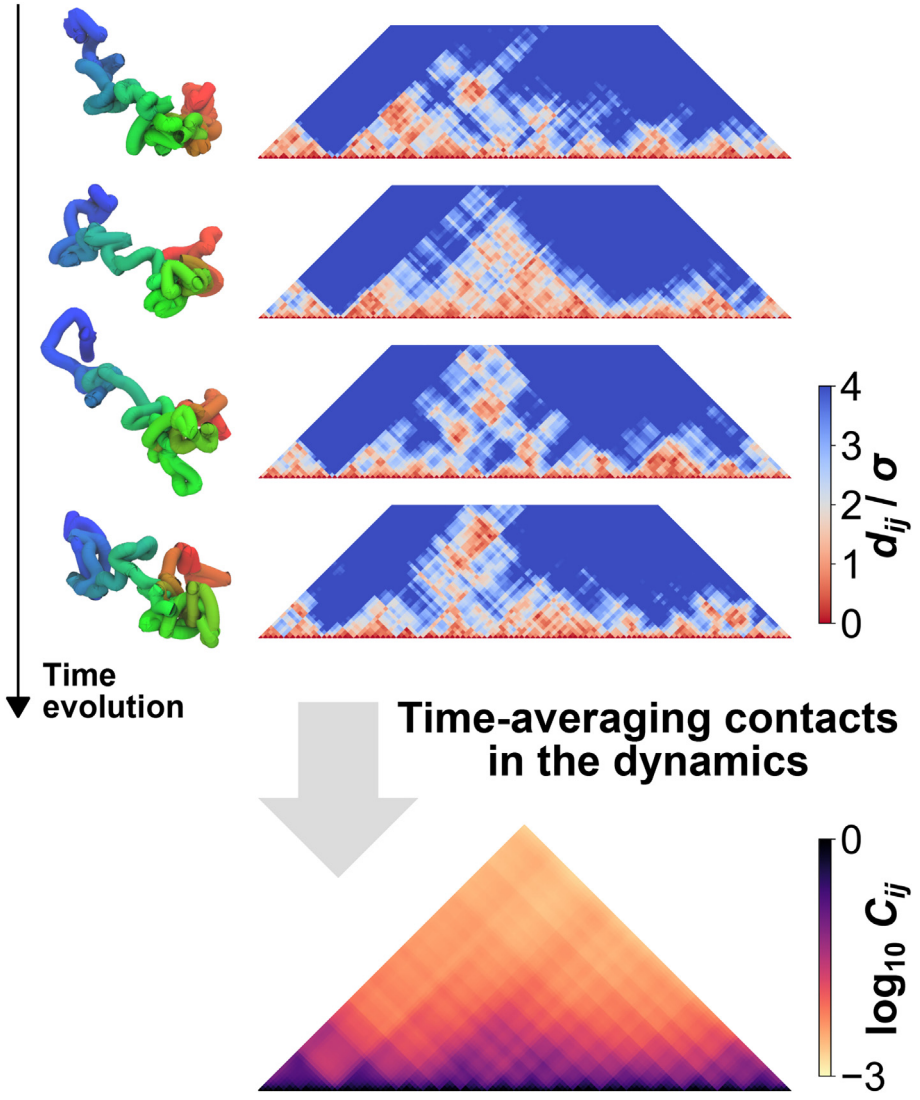

Fig. 5. PHi-C's 4D simulation yields the time-averaged contact matrix. For a polymer conformation at each time frame in a 4D simulation, the distance map is shown as a heat map of the normalized distance matrix (d_{ij}/σ). Gathering the contacts in the dynamics generates a time-averaged contact matrix. We used the optimized interaction matrix K for WT cells in Fig. 4A, calculated the 4D simulation and the distance maps, and depicted the optimized. contact matrix.

advances in super-resolution chromatin imaging of fixed cells have revealed the physical 3D conformations of labeled chromatin domains in a few hundred kb sizes [53,54]. Furthermore, super-resolution chromatin tracing reveals TAD-like structures, which are separated globules in single cells, and the sum of the contacts in the 3D conformations is consistent with population-averaged Hi-C data [55,56]. Although TADs have often been depicted as distinct, separate globules in schematic figures (Fig. 6A), it is unclear what is a structural feature of TADs in microscope observations [54]. Interestingly, the snapshots by cryo-electron microscopy (EM) [57,58] and EM tomography [59] techniques reveal not distinct chromatin globules but rather irregularly folded chromatin fibers. Furthermore, in living cells, super-resolution single-nucleosome imaging has unveiled the dynamic organization of chromatin domains [37]. Single nucleosomes mainly driven by thermal fluctuations move around within regions of a few hundred nanometers for a few seconds at a time. Therefore, without a distinct, separated globular organization, chromatin domains would be dynamically organized and behave with liquid-like properties [60–62].

Using PHi-C with microrheology analysis to process Hi-C data, we figured out that TAD boundaries are more rigid as nodes than intra-TAD sequences [16]. Relatively less mobility at the boundaries due to the rigidity than in the interior can interfere with interdomain interactions between adjacent domains. Besides, as we can infer the spatial hierarchy from the Hi-C contact map, we revealed the existence of the temporal hierarchy of genome organization. The genomic position of rigid boundaries depends on the time evolution of chromatin dynamics. Therefore, here, we propose that functional chromatin domains emerge during dynamic fluctuations within a particular time interval (Fig. 6B). Notably, this dynamic picture does not rely on the assumption of the existence of globular chromatin domains and, therefore, can reconcile bulk-based ensemble-averaged Hi-C data and dynamic genome organization in living single cells.

5. Summary and outlook

In this review, we have provided an overview of how the PHi-C modeling method deciphers Hi-C data and incorporates it into the concept of the dynamic 3D genome organization in a state undergoing thermal fluctuations. Without inferring static 3D genome structures, the PHi-C optimization procedure generated a contact

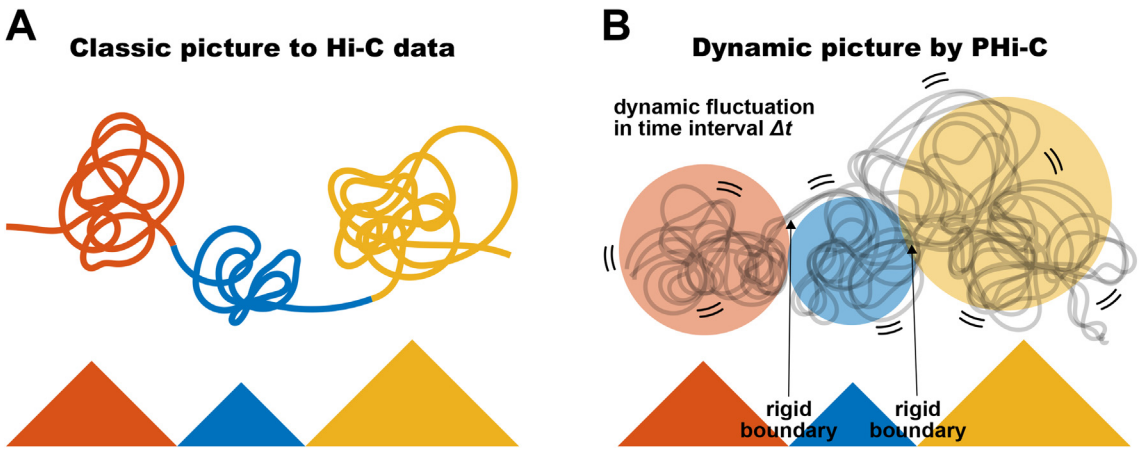

Fig. 6. Schematic illustrations for understanding the dynamic organization of chromatin domains. A, Classic picture of Hi-C data depicts distinct and separated globules corresponding to genomic triangles in a Hi-C matrix. **B**, Dynamic picture by PHi-C depicts the emergence of chromatin domains during fluctuations within a time interval Δt. The domain boundaries are more rigid, with less mobility than the interior, and can interfere with interdomain interactions.

matrix in good agreement with an input Hi-C matrix (Fig. 3), and the optimized interaction matrix of the polymer model provided the dynamic features of the 3D genomic organization (Fig. 2). As the stochastic movements of single nucleosomes and genomic loci are visible within the range of a few hundred nanometers in living cell nuclei [36,37,63–65], the PHi-C analysis was able to describe and depict the dynamic nature of chromatin. For example, a live-cell imaging experiment showed a marked difference in the movements of *Nanog* and *Oct4* loci in mouse embryonic stem cells (mESCs) [66]. Our PHi-C analysis of the two genomic loci yielded a consistent result that reflected the difference and revealed that the genomic region around *Nanog* adopts a more compact organization than the region around *Oct4* [15]. However, the physical parameters representing the spatial and temporal scales could not be determined by PHi-C analysis. Linking Hi-C data with the dynamic genomic movements in living cells is necessary for improving the PHi-C method.

The PHi-C analysis method is a post-Hi-C processing pipeline and is independent of bioinformatic analysis as it generates Hi-C matrix data from sequence data. Interestingly, with respect to defining the contacts of our polymer model, the normalization condition that the contact probability of the diagonal elements satisfies $C_{ii} = 1$ may be a new criterion for evaluating the quality of Hi-C experiments. For an experiment assessing the physical properties of a chromatin fiber, the contact frequencies along the genome coordinate within a single chromosome should be constant. We recommend combining our method with other normalization techniques to reduce and eliminate experimental biases [67–72].

Practically, the size of an input contact matrix in the PHi-C pipeline depends on the sequencing depth and binning size of the matrix. In our polymer model, we assume that the single chromatin polymer is in thermal equilibrium. Therefore, the ensemble-averaged contact probability possesses quantitative meaning, and the contact matrix is not sparse but dense. According to the sequencing depth of the Hi-C experiment, an input contact matrix should be adjusted so that the matrix is as dense as possible. Moreover, the computational cost of the PHi-C optimization procedure is proportional to $O\left(N^2\right)$ due to the iterative adjustments by random choice of matrix elements. So far, a 500×500-sized matrix is a practical upper limit for obtaining an optimized solution within a few days. The theoretical formalism and computational methods for sparse and large-sized contact matrices still require improvement.

Although 3C-based techniques have unveiled the role of 3D genome organization in diverse biological activities, our picture of the emergence of chromatin domains illustrates that the rheological rigidity at the boundaries along the 1D genome coordinate could regulate the formation of chromatin domains without the loop extrusion mechanism. Physical features such as chromatin domains must be regulated as a result of molecular orchestration on chromatin. Chromatin stiffness may create insulation at TAD boundaries [11]. Therefore, further studies are needed to elucidate how molecular interactions involving chromatin can regulate the physical stiffness and mobility of the genome. Of additional importance is the viewpoint that chromatin itself is a heterogeneous reaction field. Recently, quantitative live-imaging methods showed that intra-domain enhancer-promoter communication occurs in the absence of TADs, suggesting that boundary elements cause distal enhancers to activate target promoters independently of TAD formation in *Drosophila* embryos [73]. In mESCs, direct enhancer-promoter proximity does not drive contemporaneous *Sox2* transcription [65]. High enrichment not only of cohesin and CTCF but also of many other regulatory proteins at TAD boundaries might facilitate the formation of a local reaction field such as a transcription hub [73]. The nucleation mechanism of the reaction field might relate to liquid–liquid phase separation [74–76].

The cell-to-cell variability of chromosome structures revealed by single-cell Hi-C experiments implies that single chromosomes adopt stochastic conformations [77–79]. The summation of the conformational snapshots is consistent with the ensemble-averaged Hi-C data. Given that chromosomes are highly dynamic and that the stochastic dynamics satisfy the ergodic condition [80], PHi-C enables us to replace the ensemble-averaged Hi-C data with time-averaged data. Therefore, monitoring the spatiotemporal organization of chromatin in living cells [81] could provide consistent information about the Hi-C data of fixed cells. To understand the nature of the dynamic 3D genome, we need developments of labeling and seeing multi genomic loci with functional activities such as transcription in living cells. Mechanical manipulation and perturbation to a genomic locus could also uncover rheological features of the dynamic 3D genome. Our PHi-C model may bridge the gap between live-cell imaging and Hi-C data, contributing to the physical understanding of the dynamic 3D genome organization.

Author contributions

SS analyzed Hi-C data and generated the figures, with contributions from all authors. SS, SO, and RN wrote the manuscript.

CRediT authorship contribution statement

Soya Shinkai: Conceptualization, Methodology, Software, Data curation, Investigation, Visualization, Writing - original draft. **Shuichi Onami:** Supervision, Project administration, Writing - review & editing, Funding acquisition. **Ryuichiro Nakato:** Conceptualization, Data curation, Writing - original draft, Funding acquisition.

Declaration of Competing Interest

The authors declare that they have no known competing financial interests or personal relationships that could have appeared to influence the work reported in this paper.

Acknowledgments

This work was supported by JSPS KAKENHI Grant Nos. JP18H04720 and JP20H05550 to SS, JP17H06331 to RN, JP18H05412 to SO, and JST CREST Grant No. JPMJCR1511 to SO.

References

[1] Pombo A, Dillon N. Three-dimensional genome architecture: players and mechanisms. Nat Rev Mol Cell Biol 2015;16(4):245–57.
[2] Bonev B, Cavalli G. Organization and function of the 3D genome. Nat Rev Genet 2016;17(11):661–78.
[3] McCord RP, Kaplan N, Giorgetti L. Chromosome conformation capture and beyond: Toward an integrative view of chromosome structure and function. Mol Cell 2020;77(4):688–708.
[4] Monahan K, Horta A, Lomvardas S. LHX2- and LDB1-mediated trans interactions regulate olfactory receptor choice. Nature 2019;565 (7740):448–53.
[5] Canela A, Maman Y, Jung S, Wong N, Callen E, Day A, Kieffer-Kwon KR, Pekowska A, Zhang H, Rao SSP, Huang SC, McKinnon PJ, Aplan PD, Pommier Y, Aiden EL, Casellas R, Nussenzweig A. Genome organization drives chromosome fragility. Cell 2017;170(3):507–521.e18.
[6] Hug CB, Grimaldi AG, Kruse K, Vaquerizas JM. Chromatin architecture emerges during zygotic genome activation independent of transcription. Cell 2017;169 (2):216–228.e19.
[7] Hnisz D, Schuijers J, Li CH, Young RA. Regulation and dysregulation of chromosome structure in cancer. Ann Rev Cancer Biol 2018;2(1):21–40.
[8] Lupiáñez DG, Spielmann M, Mundlos S. Breaking TADs: how alterations of chromatin domains result in disease. Trends Genet 2016;32(4):225–37.
[9] Chakraborty A, Ay F. The role of 3D genome organization in disease: From compartments to single nucleotides. Sem Cell Develop Biol 2019;90:104–13.
[10] Lieberman-Aiden E, van Berkum NL, Williams L, Imakaev M, Ragoczy T, Telling A, Amit I, Lajoie BR, Sabo PJ, Dorschner MO, Sandstrom R, Bernstein B, Bender MA, Groudine M, Gnirke A, Stamatoyannopoulos J, Mirny LA, Lander ES, Dekker J. Comprehensive mapping of long-range interactions reveals folding principles of the human genome. Science 2009;326(5950):289–93.
[11] Dixon J, Gorkin D, Ren B. Chromatin domains: The unit of chromosome organization. Mol Cell 2016;62(5):668–80.
[12] Goloborodko A, Imakaev MV, Marko JF, Mirny L. Compaction and segregation of sister chromatids via active loop extrusion. eLife 2016;5: e14864.
[13] Terakawa T, Bisht S, Eeftens JM, Dekker C, Haering CH, Greene EC. The condensin complex is a mechanochemical motor that translocates along DNA. Science 2017;358(6363):672–6.
[14] Kim Y, Shi Z, Zhang H, Finkelstein IJ, Yu H. Human cohesin compacts DNA by loop extrusion. Science 2019;366(6471):1345–9.
[15] Shinkai S, Nakagawa M, Sugawara T, Togashi Y, Ochiai H, Nakato R, Taniguchi Y, Onami S. PHi-C: deciphering Hi-C data into polymer dynamics. NAR Genom Bioinf 2020;2(2). lqaa020.
[16] Shinkai S, Sugawara T, Miura H, Hiratani I, Onami S. Microrheology for Hi-C data reveals the spectrum of the dynamic 3D genome organization. Biophys J 2020;118(9):2220–8.
[17] Flemming W. Zellsubstantz, Kern und Zelltheilung. Vogel: F.C.W; 1882.
[18] Cremer T, Cremer M. Chromosome territories. Cold Spring Harbor Persp Biol 2010;2(3): a003889.
[19] van den Engh G, Sachs R, Trask B. Estimating genomic distance from DNA sequence location in cell nuclei by a random walk model. Science 1992;257 (5075):1410–2.
[20] Doi M, Edwards SF. The theory of polymer dynamics. Oxford University Press; 1988.
[21] Tiana G, Giorgetti L, editors. Modeling the 3D conformation of Genomes. CRC Press; 2019.
[22] Merlotti A, Rosa A, Remondini D. Merging 1D and 3D genomic information: Challenges in modelling and validation. Biochim Biophys Acta (BBA) – Gene Regul Mech 2020;1863(6):194415.
[23] Brackey CA, Marenduzzo D, Gilbert N. Mechanistic modeling of chromatin folding to understand function. Nat Methods 2020;17:767–75.
[24] Münkel C, Langowski J. Chromosome structure predicted by a polymer model. Phys Rev E 1998;57:5888–96.
[25] Rosa A, Everaers R. Structure and dynamics of interphase chromosomes. PLOS Comput Biol 2008;4(8):1–10.
[26] Barbieri M, Chotalia M, Fraser J, Lavitas L-M, Dostie J, Pombo A, Nicodemi M. Complexity of chromatin folding is captured by the strings and binders switch model. Proc Natl Acad Sci USA 2012;109(40):16173–8.
[27] Brackley CA, Taylor S, Papantonis A, Cook PR, Marenduzzo D. Nonspecific bridging-induced attraction drives clustering of DNA-binding proteins and genome organization. Proc Natl Acad Sci USA 2013;110(38):E3605–11.
[28] Jost D, Carrivain P, Cavalli G, Vaillant C. Modeling epigenome folding: formation and dynamics of topologically associated chromatin domains. Nucleic Acids Res 2014;42(15):9553–61.
[29] Fudenberg G, Imakaev M, Lu C, Goloborodko A, Abdennur N, Mirny LA. Formation of chromosomal domains by loop extrusion. Cell Rep 2016;15 (9):2038–49.
[30] Kempfer R, Pombo A. Methods for mapping 3D chromosome architecture. Nat Rev Genet 2020;21(4):207–26.
[31] Giorgetti L, Heard E. Closing the loop: 3C versus DNA FISH. Genome Biol 2016;17(1):215.
[32] Fudenberg G, Imakaev M. FISH-ing for captured contacts: towards reconciling FISH and 3C. Nat Methods 2017;14:673–8.
[33] Serra F, Di Stefano M, Spill YG, Cuartero Y, Goodstadt M, Baú D, Marti-Renom MA. Restraint-based three-dimensional modeling of genomes and genomic domains. FEBS Lett 2015;589(20 PartA):2987–95.
[34] Le Treut G, Képès F, Orland H. A polymer model for the quantitative reconstruction of chromosome architecture from HiC and GAM data. Biophys J 2018;115(12):2286–94.
[35] Liu L, Kim MH, Hyeon C. Heterogeneous loop model to infer 3D chromosome structures from Hi-C. Biophys J 2019;117(3):613–25.
[36] Shinkai S, Nozaki T, Maeshima K, Togashi Y. Dynamic nucleosome movement provides structural information of topological chromatin domains in living human cells. PLOS Comput Biol 2016;12(10): e1005136.
[37] Nozaki T, Imai R, Tanbo M, Nagashima R, Tamura S, Tani T, Joti Y, Tomita M, Hibino K, Kanemaki MT, Wendt KS, Okada Y, Nagai T, Maeshima K. Dynamic organization of chromatin domains revealed by super-resolution live-cell imaging. Mol Cell 2017;67(2):282–293.e7.
[38] Marti-Renom MA, Mirny LA. Bridging the resolution gap in structural modeling of 3D genome organization. PLOS Comput Biol 2011;7(7): e1002125.
[39] Shinkai S, Nozaki T, Maeshima K, Togashi Y. Bridging the dynamics and organization of chromatin domains by mathematical modeling. Nucleus 2017;8(4):353–9.
[40] Gardiner C. Stochastic Methods. 4th ed. Berlin Heidelberg: Springer-Verlag; 2009.
[41] Mason TG, Weitz DA. Optical measurements of frequency-dependent linear viscoelastic moduli of complex fluids. Phys Rev Lett 1995;74:1250–3.
[42] Giorgetti L, Galupa R, Nora E, Piolot T, Lam F, Dekker J, Tiana G, Heard E. Predictive polymer modeling reveals coupled fluctuations in chromosome conformation and transcription. Cell 2014;157(4):950–63.
[43] Zhang B, Wolynes PG. Topology, structures, and energy landscapes of human chromosomes. Proc Natl Acad Sci USA 2015;112(19):6062.
[44] Di Pierro M, Zhang B, Aiden EL, Wolynes PG, Onuchic JN. Transferable model for chromosome architecture. Proc Natl Acad Sci USA 2016;113(43):12168.
[45] Chiariello AM, Annunziatella C, Bianco S, Esposito A, Nicodemi M. Polymer physics of chromosome large-scale 3D organisation. Sci Rep 2016;6 (1):29775.
[46] Bianco S, Lupiáñez DG, Chiariello AM, Annunziatella C, Kraft K, Schöpflin R, Wittler L, Andrey G, Vingron M, Pombo A, Mundlos S, Nicodemi M. Polymer physics predicts the effects of structural variants on chromatin architecture. Nat Genet 2018;50(5):662–7.
[47] Fudenberg G, Abdennur N, Imakaev M, Goloborodko A, Mirny LA. Emerging evidence of chromosome folding by loop extrusion. Cold Spring Harb Symp Quant Biol 2017;82:45–55.
[48] Gibcus JH, Samejima K, Goloborodko A, Samejima I, Naumova N, Nuebler J, Kanemaki MT, Xie L, Paulson JR, Earnshaw WC, Mirny LA, Dekker J. A pathway for mitotic chromosome formation. Science 2018;359(6376). eaao6135.
[49] Zuin J, Dixon JR, van der Reijden MIJA, Ye Z, Kolovos P, Brouwer RWW, van de Corput MPC, van de Werken HJG, Knoch TA, van IJcken WFJ, Grosveld FG, Ren B, Wendt KS. Cohesin and CTCF differentially affect chromatin architecture and gene expression in human cells. Proc Natl Acad Sci USA 2014;111(3):996.
[50] Nora EP, Goloborodko A, Valton A-L, Gibcus JH, Uebersohn A, Abdennur N, Dekker J, Mirny LA, Bruneau BG. Targeted degradation of CTCF decouples local insulation of chromosome domains from genomic compartmentalization. Cell 2017;169(5):930–944.e22.
[51] Haarhuis JHI, van der Weide RH, Blomen VA, Yáñez-Cuna JO, Amendola M, van Ruiten MS, Krijger PHL, Teunissen H, Medema RH, van Steensel B, Brummelkamp TR, de Wit E, Rowland BD. The cohesin release factor WAPL restricts chromatin loop extension. Cell 2017;169(4):693–707.e14.
[52] Wutz G, Várnai C, Nagasaka K, Cisneros DA, Stocsits RR, Tang W, Schoenfelder S, Jessberger G, Muhar M, Hossain MJ, Walther N, Koch B, Kueblbeck M, Ellenberg J, Zuber J, Fraser P, Peters J-M. Topologically associating domains and chromatin loops depend on cohesin and are regulated by CTCF, WAPL, and PDS5 proteins. EMBO J 2017;36(24):3573–99.

[53] Boettiger AN, Bintu B, Moffitt JR, Wang S, Beliveau BJ, Fudenberg G, Imakaev M, Mirny LA, Wu C-T, Zhuang X. Super-resolution imaging reveals distinct chromatin folding for different epigenetic states. Nature 2016;529 (7586):418–22.
[54] Boettiger A, Murphy S. Advances in chromatin imaging at kilobase-scale resolution. Trends Genet 2020;36(4):273–87.
[55] Bintu B, Mateo LJ, Su J-H, Sinnott-Armstrong NA, Parker M, Kinrot S, Yamaya K, Boettiger AN, Zhuang X. Super-resolution chromatin tracing reveals domains and cooperative interactions in single cells. Science 2018;362(6413). eaau1783.
[56] Mateo LJ, Murphy SE, Hafner A, Cinquini IS, Walker CA, Boettiger AN. Visualizing DNA folding and RNA in embryos at single-cell resolution. Nature 2019;568(7750):49–54.
[57] Eltsov M, MacLellan KM, Maeshima K, Frangakis AS, Dubochet J. Analysis of cryo-electron microscopy images does not support the existence of 30-nm chromatin fibers in mitotic chromosomes in situ. Proc Natl Acad Sci USA 2008;105(50):19732.
[58] Cai S, Chen C, Tan ZY, Huang Y, Shi J, Gan L. Cryo-ET reveals the macromolecular reorganization of *S. pombe* mitotic chromosomes in vivo. Proc Natl Acad Sci USA 2018;115(43):10977.
[59] Ou HD, Phan S, Deerinck TJ, Thor A, Ellisman MH, O'Shea CC. ChromEMT: Visualizing 3D chromatin structure and compaction in interphase and mitotic cells. Science 2017;357(6349). eaag0025.
[60] Maeshima K, Hihara S, Eltsov M. Chromatin structure: does the 30-nm fibre exist in vivo? Curr Opin Cell Biol 2010;22(3):291–7.
[61] Maeshima K, Ide S, Hibino K, Sasai M. Liquid-like behavior of chromatin. Curr Opin Genet Devel 2016;37:36–45.
[62] Maeshima K, Tamura S, Hansen JC, Itoh Y. Fluid-like chromatin: Toward understanding the real chromatin organization present in the cell. Curr Opin Cell Biol 2020;64:77–89.
[63] Germier T, Kocanova S, Walther N, Bancaud A, Shaban HA, Sellou H, Politi AZ, Ellenberg J, Gallardo F, Bystricky K. Real-time imaging of a single gene reveals transcription-initiated local confinement. Biophys J 2017;113(7):1383–94.
[64] Amitai A, Seeber A, Gasser SM, Holcman D. Visualization of chromatin decompaction and break site extrusion as predicted by statistical polymer modeling of single-locus trajectories. Cell Rep 2017;18(5):1200–14.
[65] Alexander JM, Guan J, Li B, Maliskova L, Song M, Shen Y, Huang B, Lomvardas S, Weiner OD. Live-cell imaging reveals enhancer-dependent *Sox2* transcription in the absence of enhancer proximity. eLife 2019;8: e41769.
[66] Ochiai H, Sugawara T, Yamamoto T. Simultaneous live imaging of the transcription and nuclear position of specific genes. Nucleic Acids Res 2015;43(19):e127.
[67] Yaffe E, Tanay A. Probabilistic modeling of Hi-C contact maps eliminates systematic biases to characterize global chromosomal architecture. Nat Genet 2011;43(11):1059–65.
[68] Hu M, Deng K, Selvaraj S, Qin Z, Ren B, Liu JS. HiCNorm: removing biases in Hi-C data via Poisson regression. Bioinformatics 2012;28(23):3131–3.
[69] Imakaev M, Fudenberg G, McCord RP, Naumova N, Goloborodko A, Lajoie BR, Dekker J, Mirny LA. Iterative correction of Hi-C data reveals hallmarks of chromosome organization. Nat Methods 2012;9:999–1003.
[70] Knight PA, Ruiz D. A fast algorithm for matrix balancing. IMA J Numer Anal 2012;33(3):1029–47.
[71] Rao SP, Huntley M, Durand N, Stamenova E, Bochkov I, Robinson J, Sanborn A, Machol I, Omer A, Lander E, Aiden E. A 3D map of the human genome at kilobase resolution reveals principles of chromatin looping. Cell 2014;159 (7):1665–80.
[72] Spill YG, Castillo D, Vidal E, Marti-Renom MA. Binless normalization of Hi-C data provides significant interaction and difference detection independent of resolution. Nat Commun 2019;10(1):1938.
[73] Yokoshi M, Segawa K, Fukaya T. Visualizing the role of boundary elements in enhancer-promoter communication. Mol Cell 2020;78(2):224–235.e5.
[74] Brangwynne C, Tompa P, Pappu R. Polymer physics of intracellular phase transitions. Nat Phys 2015;11(11):899–904.
[75] Shin Y, Chang Y-C, Lee DSW, Berry J, Sanders DW, Ronceray P, Wingreen NS, Haataja M, Brangwynne CP. Liquid nuclear condensates mechanically sense and restructure the genome. Cell 2018;175(6):1481–1491.e13.
[76] Larson AG, Elnatan D, Keenen MM, Trnka MJ, Johnston JB, Burlingame AL, Agard DA, Redding S, Narlikar GJ. Liquid droplet formation by HP1α suggests a role for phase separation in heterochromatin. Nature 2017;547(7662):236–40.
[77] Nagano T, Lubling Y, Stevens TJ, Schoenfelder S, Yaffe E, Dean W, Laue ED, Tanay A, Fraser P. Single-cell Hi-C reveals cell-to-cell variability in chromosome structure. Nature 2013;502(7469):59–64.
[78] Flyamer IM, Gassler J, Imakaev M, Brandão HB, Ulianov SV, Abdennur N, Razin SV, Mirny LA, Tachibana-Konwalski K. Single-nucleus Hi-C reveals unique chromatin reorganization at oocyte-to-zygote transition. Nature 2017;544 (7648):110–4.
[79] Ulianov SV, Tachibana-Konwalski K, Razin SV. Single-cell Hi-C bridges microscopy and genome-wide sequencing approaches to study 3D chromatin organization. BioEssays 2017;39(10):1700104.
[80] Dekker J. Chromosome folding: Contributions of chromosome conformation capture and polymer physics. In: Tiana G, Giorgetti L, editors. Modeling the 3D conformation of genomes. CRC Press; 2019. p. 1–17.
[81] Shaban HA, Seeber A. Monitoring the spatio-temporal organization and dynamics of the genome. Nucleic Acids Res 2020;48(7):3423–34.
[82] Mateos-Langerak J, Bohn M, de Leeuw W, Giromus O, Manders EMM, Verschure PJ, Indemans MHG, Gierman HJ, Heermann DW, van Driel R, Goetze S. Spatially confined folding of chromatin in the interphase nucleus. Proc Natl Acad Sci USA 2009;106(10):3812–7.
[83] Tokuda N, Terada T, Sasai M. Dynamical modeling of three-dimensional genome organization in interphase budding yeast. Biophys J 2012;102 (2):296–304.